**Article:**
Lord, Alex M, Ramasse, Quentin M, Kepaptsoglou, Despoina M orcid.org/0000-0003-0499-0470 et al. (3 more authors) (2017) Stability of Schottky and Ohmic Au Nanocatalysts to ZnO Nanowires. Nano Letters. pp. 6626-6636. ISSN 1530-6984

https://doi.org/10.1021/acs.nanolett.7b02561

NANO LETTERS

Letter

Cite This: Nano Lett. 2017, 17, 6626-6636

pubs.acs.org/NanoLett

# Stability of Schottky and Ohmic Au Nanocatalysts to ZnO Nanowires

Alex M. Lord,[*,†] Quentin M. Ramasse,[‡] Despoina M. Kepaptsoglou,[‡] Priyanka Periwal,[§,∥] Frances M. Ross,[∥] and Steve P. Wilks[⊥]

[†]Centre for NanoHealth, College of Engineering, University of Swansea, Singleton Park SA2 8PP, United Kingdom

[‡]SuperSTEM Laboratory, SciTech Daresbury Campus, Keckwick Lane, Daresbury WA4 4AD, United Kingdom

[§]Department of Electrical Engineering, University of Cambridge, Cambridge CB0 3FA, United Kingdom

[∥]IBM T. J. Watson Research Center, Yorktown Heights, New York 10598, United States of America

[⊥]Multidisciplinary Nanotechnology Centre, Department of Physics, College of Science, University of Swansea, Singleton Park, SA2 8PP, United Kingdom

Supporting Information

**ABSTRACT:** Manufacturable nanodevices must now be the predominant goal of nanotechnological research to ensure the enhanced properties of nanomaterials can be fully exploited and fulfill the promise that fundamental science has exposed. Here, we test the electrical stability of Au nanocatalyst−ZnO nanowire contacts to determine the limits of the electrical transport properties and the metal−semiconductor interfaces. While the transport properties of as-grown Au nanocatalyst contacts to ZnO nanowires have been well-defined, the stability of the interfaces over lengthy time periods and the electrical limits of the ohmic or Schottky function have not been studied. In this work, we use a recently developed iterative analytical process that directly correlates multiprobe transport measurements with subsequent aberration-corrected scanning transmission electron microscopy to study the electrical, structural, and chemical properties when the nanowires are pushed to their electrical limits and show structural changes occur at the metal−nanowire interface or at the nanowire midshaft. The ohmic contacts exhibit enhanced quantum-mechanical edge-tunneling transport behavior because of additional native semiconductor material at the contact edge due to a strong metal−support interaction. The low-resistance nature of the ohmic contacts leads to catastrophic breakdown at the middle of the nanowire span where the maximum heating effect occurs. Schottky-type Au−nanowire contacts are observed when the nanowires are in the as-grown pristine state and display entirely different breakdown characteristics. The higher-resistance rectifying $I-V$ behavior degrades as the current is increased which leads to a permanent weakening of the rectifying effect and atomic-scale structural changes at the edge of the Au interface where the tunneling current is concentrated. Furthermore, to study modified nanowires such as might be used in devices the nanoscale tunneling path at the interface edge of the ohmic nanowire contacts is removed with a simple etch treatment and the nanowires show similar $I-V$ characteristics during breakdown as the Schottky pristine contacts. Breakdown is shown to occur either at the nanowire midshaft or at the Au contact depending on the initial conductivity of the Au contact interface. These results demonstrate the Au−nanowire structures are capable of withstanding long periods of electrical stress and are stable at high current densities ensuring they are ideal components for nanowire-device designs while providing the flexibility of choosing the electrical transport properties which other Au−nanowire systems cannot presently deliver.

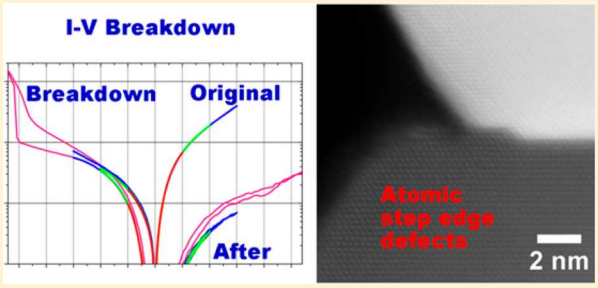


**KEYWORDS:** *Nanowires, electrical contacts, tunneling edge effect, aberration-corrected scanning transmission electron microscopy, electrical breakdown, barrier inhomogeneity, interfacial atomic defects, ZnO*

Recent advances in experimental and analytical techniques have allowed researchers to investigate the limits within which nanostructures can operate. These investigations are essential to determine that they can provide consistent performance throughout their operational lifetime and therefore better define their suitability in future applications. The mechanical, structural, and electrical breakdown of many nanostructured materials such as graphene[1] have been studied by a range of techniques. Similarly, remarkable effects in one-dimensional (1D) nanomaterials have been reported such as the migration of the Au catalyst materials through the bulk of Ge and GaAs nanowires[2,3] and away from the tip of Si nanowires to control the Au shape.[4,5] In situ transmission electron microscopy (TEM) has been used to investigate the breakdown of Joule heated GaN nanowires,[6,7] modification of InAs/InGaAs nanowires,[8,9] heating of nanotubes,[10−12] and interfacial effects in charge storage materials.[13]

**Received:** June 16, 2017
**Revised:** September 19, 2017
**Published:** October 12, 2017




DOI: 10.1021/acs.nanolett.7b02561
Nano Lett. 2017, 17, 6626−6636

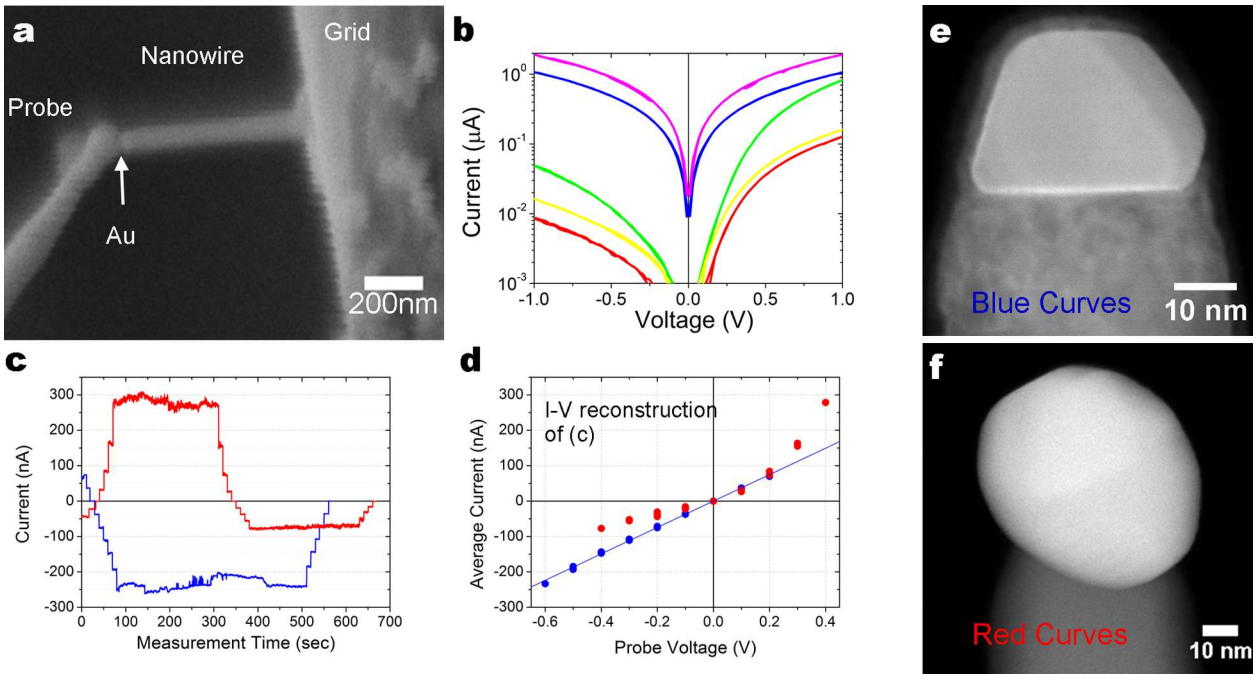


**Figure 1.** (a) In situ SEM image from the multiprobe UHV instrument used to measure the nanowires in the eSTEM cantilever configuration displaying the tungsten measurement probe, the nanowire, and Au nanocontact at the nanowire tip. (b) A graph showing *I*−*V* measurements of two chronologically aged ohmic nanowires (blue, purple) and three pristine as-grown Schottky-type nanowires (green, yellow, red) in the eSTEM configuration. (c) Current−time (*I*−*t*) measurements testing the electrical stability of a chronologically aged Au−ZnO (blue) and a freshly grown interface (red). The *I*−*t* plot from the measurement of the aged nanowire in the eSTEM configuration shows 0.1 V steps from 0.2 to −0.6 V and the return steps to 0 V. The freshly grown nanowire similarly shows 0.1 V steps from −0.2 V to 0.4 V with a constant bias regime of 200 s and then voltage steps 0.4 V to −0.4 V with a 200 s dwell before the 0.1 V stepped return to 0 V. (d) Reconstructed current−voltage plot where each current value is the average from each voltage step for the entire *I*−*t* measurements in (c) including the up and down voltage ramps (the current at each voltage step overlap for each voltage ramp up and down indicating no change in the contact properties even after the prolonged dwell time at maximum current). (e) ac-STEM MAADF image of the chronologically aged ohmic nanowire corresponding to the blue data in (b−d). (f) ac-STEM HAADF image of the freshly grown Schottky nanowire corresponding to the red data in (b−d).

The Au nanoparticle catalyst that promotes the growth of many nanowires removes any need for postgrowth processing to create complete devices.[4] Recent work on Au nanocontacts to ZnO nanowires has shown that the transport properties can be switched from ohmic to Schottky as a result of quantum-mechanical edge-tunneling effects by selecting a nanocontact that is comparable in diameter to the nanowire or by modifying the semiconductor material near the interface edge.[14,15] Currently, the Au catalyst−ZnO nanowire system is the only known material that exhibits quantum-mechanical edge tunneling in such a way that the effect can be used to modulate the transport properties from Schottky to ohmic. Other typical nanowire materials grown with Au nanocatalysts exhibit only ohmic behavior such as silicon nanowires[4,5] or the strongly rectifying properties of GaAs and Ge nanowires.[16,17] Several attempts have been made to tailor the transport properties of Au catalyst growth particles applied as electrical contacts on the tips of nanowires including traditional bulk or planar contact modifications such as changes in the interface dipole that can be achieved by metal alloying or heterostructure formation.[16] However, more recent advances applying the fundamental quantum or nanometric properties of nanomaterials have allowed size effects to modulate carrier transport in addition to atomic- and nanoscale changes to the semiconductor material near the interface edge.[14−17] The technique for modifying the atomic or nanoscale structure and chemistry of the interface edge-region holds great promise because it can be exploited by a number of methods such as etching,[18,19] nanowire surface/interface architecture modulation during growth,[20,21] or the addition of nanowire shell materials.[22−25] This flexibility provides great potential for selecting the exact properties of individual nanowires, nanodevices, and the electrical contacts that integrate the two. Crucially, there has been little detailed study of the resilience and stability of the Au particles as electrical contacts even though much work has been focused on the fundamental growth, catalytic, and electrical properties of the 1D nanostructures after growth while the catalytic processes that governs their formation are subject to ongoing studies at the atomic-level in real-time.[18,21,26−31]

In this work, we investigate ZnO nanowires with low-resistance ohmic Au nanocatalyst growth particles as electrical contacts that have been modified from their as-grown state by a strong metal−support interaction (SMSI) that encapsulates the Au contacts adding defective native ZnO material to the edge region and creating ohmic transport behavior because of the enhanced tunneling path. These nanowires are compared to similarly grown nanowires with Au contacts exhibiting rectifying behavior that are in the initial nonaged state with no evidence of SMSI and no extraneous ZnO material at the interface edge.[15] The transport properties of the Au contacts to ZnO nanowires are governed by an edge-tunneling phenomenon that can be modulated through nanoscale modification to the ZnO n-type semiconductor near the Au nanocatalyst particle−nanowire interface edge. Thus, there is a requirement to examine the difference in the capabilities of the two nanowire types to assess their suitability for real devices. In



DOI: 10.1021/acs.nanolett.7b02561
*Nano Lett.* 2017, 17, 6626−6636

comparison to the ohmic and Schottky contacts, the edge-tunneling path at the edge of the contacts in the ohmic aged SMSI nanowires are modified by etching away the extraneous ZnO material that produces a range of transport behavior that is governed by the central interface rather than the edge. Transport in the modified nanowires is dominated by the nature of the central interface that creates high-resistance contacts providing a direct comparison to the Schottky and ohmic nanowires where edge tunneling prevails. Here, we test this range of electrical contacts with multiprobe electrical transport measurements and correlate this behavior directly to aberration-corrected scanning transmission electron microscopy (ac-STEM) on the same nanowires to show ZnO nanomaterials are suitable as robust electrical components for nanodevices. Initially, the nanowires are tested for long-periods of applied current in the expected operational current range (±300 nA) because any nanodevice material should provide consistent performance over lengthy periods. This work goes on to show that the low-resistance ohmic contacts, pristine Schottky contacts, and high-resistance etched contacts are robust nanodevice components and the electrical limits are tested to breakdown which is shown to occur either at the nanowire midshaft or through atomic-scale defect formation at the Au contact edge depending on the Au−ZnO interface conductivity. The demonstrated effects show that the Au−ZnO nanowire structures are undoubtedly prime candidates for stable devices and the reported behavior suggests a vast range of capabilities ripe for commercialization when the correct R&D resources are in place.[16,32]

**Results and Discussion.** *Electrical Measurement and ac-STEM Experimental Process.* Addition of native ZnO material to the contact edge region was achieved by a strong metal interaction between the Au catalyst and ZnO nanowire.[14] This occurred as a chronological aging process of the ZnO nanowires that were grown by a metal-catalyzed vapor phase technique[33] and stored for ∼3 years in ambient laboratory conditions. The nanowires were then mechanically transferred to a standard copper 4-post focused ion-beam TEM lift-out grid without any further treatment. The grids were screened in a conventional TEM to locate overhanging nanowires that had the Au−ZnO interface close to parallel with the electron beam and to capture the initial state of the nanowires (Figure S1a) before the first iteration of electrical transport measurements. The preparation technique of transferring the nanowires to the grid provides a ZnO coating of base growth material to the copper grid ensuring the nanowire−ZnO−Cu interface is ohmic in nature (Figure S1b).[14,34] The experimental (eSTEM) procedure has been previously described and was employed here in a similar fashion to initially apply an ultrahigh vacuum (UHV) multiprobe scanning tunneling microscopy (STM) instrument with in situ SEM capability to measure the transport behavior of the nanowires suspended on the grid (Figure 1a).[14] The multiprobe instrument allowed a tungsten probe to be maneuvered with nanometer precision such that it could be accurately placed onto the Au tips of the overhanging ZnO nanowires (Figure 1a). Performing the electrical measurements in the UHV-STM instrument provided the advantage that the tungsten measurement probes could be thermally annealed in situ to remove oxides and contamination ensuring the probe-to-Au contact was a low-resistance metal-on-metal contact (similar resistance to the system resistance ∼200 Ω) and as such the transport measurements revealed the properties of the Au−nanowire structures.[15,34−36]

Initial measurements tested the current−voltage characteristics ($I$−$V$) of the metal−semiconductor interfaces which is the predominant technique for revealing the behavior and performance of an electrical contact.[37] The nanowires were then removed from the UHV-STM instrument and were interrogated with aberration-corrected scanning transmission electron microscopy (ac-STEM) imaging and electron energy-loss spectroscopy (EELS) mapping, providing access to the ultimate electron microscopy "on-axis" imaging resolution and spectroscopic signal.[38] After the structural and chemical characterization, the nanowires were transferred back to the multiprobe UHV instrument, where current−time ($I$−$t$) measurements were performed on the same nanowires over extended timeframes to establish the stability of the contacts to prolonged current, in effect establishing the temporal stability of the contacts in the typical operating current range for a realistic nanodevice. After the $I$−$t$ electrical measurements, the sample grid was once more removed from the UHV multiprobe STM instrument and the same nanowires, particularly the Au interfaces, were once more interrogated with ac-STEM and EELS mapping to assess whether the extended current period had affected the Au−nanowire interfaces.

Application of the eSTEM experimental approach made it possible to perform a multistep iterative electrical measurement and electron microscopy procedure on the same nanowires before and after several electrical transport experiments, ex situ modifications, and ac-STEM/EELS analysis (a step-by-step description has been previously provided).[14] This flexible experimental process was applied in total to a relatively large number (∼35) of Au nanocontacts on ZnO nanowires. Electrical in situ probing of nanoscale materials in the TEM has produced many important recent results studying the stability of 1D nanomaterials but most are performed with metal probes that have not been annealed or require fabricated ohmic contacts and as such can only concentrate on the response of the nanomaterial to the current rather than the current−voltage behavior of the metal nanoparticle-nanowire interfaces. The technique used here provides this ability that is essential for revealing the transport properties of the Au nanocatalyst−electrical contacts.[37] A number of works have endeavored to reveal such behavior of Au−nanowire interfaces but have not allowed direct correlation to the atomic-scale interface structure and chemistry at the metal−semiconductor interfaces.[16,17,39−41] Additionally, the electrical properties of ZnO nanostructures and the nanocatalyst contacts are dominated by the surface and the materials are highly susceptible to any processing that is often necessary for in situ measurement devices.[14,15,42,43] Progressing from the $I$−$t$ and ac-STEM/EELS analysis, the nanowires were tested for their current−voltage stability with increasing applied bias sweeps and the observed changes were correlated to ac-STEM to determine the structural and chemical characteristics of the interfaces and nanowires.

*Electrical Temporal Stability of Ohmic and Schottky Au Nanocontacts to ZnO Nanowires.* Figure 1a,b presents the experimental configuration and the initial current−voltage characteristics ($I$−$V$) of a number of nanowires that revealed the contact-type transport characteristics, whether they were Schottky or ohmic.

After an initial ac-STEM characterization through imaging and spectroscopy, the electrical-temporal stability of the contacts was tested on ∼35 eSTEM ohmic and Schottky nanowire−nanocontact structures with prolonged electrical



DOI: 10.1021/acs.nanolett.7b02561
Nano Lett. 2017, 17, 6626−6636

stress by applying a range of forward- and/or reverse-bias current within the typical operational range of functional nanowire devices of a few nA to several hundred nA to test the longevity of the Au−nanowire structures by maintaining the applied bias for up to 15 min. The current−time ($I$−$t$) characteristics of a Schotty-type (red) and ohmic-type (blue) nanowire are shown in Figure 1c. Reconstructing the $I$−$V$ graph from each voltage 0.1 V step in the data showed a linear $I$−$V$ relationship for the ohmic contact, Figure 1d (blue), with the current at each step in the initial ramp from 0.2 to −0.6 V being equal to the current at each voltage step on the final ramp from −0.6 to 0 V after dwelling at ∼−250 nA for 400 s, indicating the contact was unaffected by the long measurement time or current magnitude. In a similar fashion, nonaged Schottky nanowires taken from a freshly grown nanowire array were tested in the same cantilever eSTEM configuration (Figure 1c,d) that shows the bias was ramped up and down through positive- to reverse-bias and the reconstructed $I$−$V$, Figure 1d (red), shows the nonlinear $I$−$V$ characteristics. In these experiments the focus was predominantly on the reverse-bias regime when tunneling dominates at the contact edge that creates the greatest localized current densities at the interface perimeter because of the edge-tunneling phenomenon.[15,44,45] Therefore, the interface edge-region was of particular interest during the ac-STEM analysis following our recent work that showed atomic- and nanoscale modifications to the interface edge can entirely alter the transport properties rather than the less-influential central zone of the circular Au−ZnO interfaces.[14,46] High-current densities can lead to structural breakdown, however, to ensure the complete interface was characterized the entire edge and central zone of the interfaces were scrupulously analyzed with ac-STEM to detect any structural or chemical modification.

It is noted that the rectification of the freshly grown nanowire in the $I$−$t$ measurement (Figure 1b−d,f; red data) reduced in rectification ratio and increased in conductivity after the initial ac-STEM interrogation. This is likely due to a number of effects: handling of the specimens and transfers to/from the UHV-STM chamber to the ac-STEM apparatus may have resulted in some environmental modification (deposition of adventitious carbon contamination, some surface oxidation, and so forth); furthermore, damage from exposure to the intense electron beam during ac-STEM imaging and EELS mapping (see Figure S2 for $I$−$V$ graphs before and after ac-STEM analysis recorded before the $I$−$t$ measurements) cannot be ruled out, even though before/after images showed no obvious visible structural modification. By contrast, any effect of the $I$−$V$ or $I$−$t$ measurements was ruled out by repeated $I$−$V$ sweeps at ±1 V of numerous contacts that showed no change in transport behavior and previously was shown in detail.[15] Similarly, the aged ohmic contact (Figure 1c) displayed greater current magnitude after ac-STEM analysis but retained its ohmic nature. ZnO nanowires are susceptible to beam damage that can introduce point defects in the ZnO near the interface and at the nanowire surface that can reduce contact rectification as shown by the ohmic nature of the nanowires affected by a SMSI.[14] However, the later sections of this work will show the freshly grown Schottky nanowire contacts retain their rectifying properties at greater bias and the aged ohmic contacts retain their ohmic nature and low-resistance. To provide further confirmation that the reduction in rectification may have been primarily a result of the electron analysis, a rectifying nanowire on the same sample that was not subjected to ac-STEM/EELS was measured at the end of the entire experimental process and was shown to have typical rectifying quality (see Figure S3) and additionally, aged ohmic nanowires that had not been scrutinized intensely with STEM were also ohmic.

Bright field (BF), high-angle annular dark-field (HAADF), and medium-angle annular dark-field (MAADF) ac-STEM imaging of the measured eSTEM nanowires was performed and revealed structural anomalies of the ZnO (the defective edge-region of aged nanowires was the focus of our previous work)[14] near the metal−semiconductor interface in only one of the measured nanowires, as shown in Figure S4a,b. Figure S4c shows the ZnO stacking fault originated at the Au interface where a twinning boundary in the Au occurs that was revealed by through-focal series imaging stacks. Figure S4c reveals the atomic-abruptness of the interface in the region adjacent to the twinning boundary but Figure S4b shows that a single Au atomic step occurs where the twin boundary interfaces with the nanowire and the stacking fault extends ∼2 nm into the nanowire. However, this had little effect on the electrical transport properties of the aged nanowire due to the predominance of quantum-mechanical tunneling at the interface edge. Barrier inhomogeneity is a known hindrance in ideal large-scale Schottky contacts that is often attributed to local interface variations such as defects, dopants, and contamination; however, the measurements here did not show any significant indications that this was a major factor in the electrical properties of this wire.[47] The analysis showed there was no contact, nanowire, or interface degradation in any of the 14 other nanowires that were examined "on-axis" after the $I$−$t$ measurements. However, twinning of the Au particle is a common occurrence that requires further investigation to determine the effect on the transport properties although this is expected to be minimal at low bias (±1 V) when transport is edge-tunneling dominated (a discourse on the presence of Au twins and the atomic-scale structure at the interface is provided with Supporting Information Figure S5 to S11).[14,15,29,42,45,48,49] Through-focal imaging and nanoscale EELS maps of the interface confirmed there was no Au diffusion as shown by the nanoscale EELS maps in Supporting Information Figure S12.

In summary, the analysis shows that the interface between the Au and ZnO in the central region of the contacts retained the high crystal quality and atomic abruptness that is apparent in pristine unmeasured ZnO nanowires[50] with no diffusion of Au or blurring of the interface after the initial $I$−$V$ and $I$−$t$ measurements. The lack of diffusion across the Au−nanowire interface was thoroughly investigated with through-focal sectioning that can reveal Au atoms on the surface or buried deep within the bulk using depth-slicing techniques which exploit the reduced depth of field (2−4 nm) to locally image impurities, in particular at point defects.[50,51] The crystal quality at the contact edge that was initially apparent in the ohmic contacts remained in the degraded state at the interface edge in all the aged nanowires without disruption to the enhanced quantum-mechanical tunneling channel and ohmic transport properties. The significant evidence here is the ohmic and Schottky structures maintained their original form after the $I$−$t$ measurements at the Au−nanowire interface that controls the edge-tunneling and subsequent contact transport behavior displaying that the structures are suitable device components.

*Current−Voltage Characteristics of Au Contacts on ZnO Nanowires.* The initial $I$−$V$ stability electrical measurements of the Au−nanowire interfaces involved $I$−$V$ sweeps between ±1 V of the ohmic chronologically aged nanowires in the eSTEM



DOI: 10.1021/acs.nanolett.7b02561
Nano Lett. 2017, 17, 6626−6636

configuration that showed a range of current magnitude from several tens of nA to a few $\mu$A and displayed linear ohmic-like $I-V$ characteristics for the 15 nanowires that were measured, Figure 1b. The ohmic behavior was previously confirmed with two-probe measurements on free-standing nanowires and similarly, freshly grown nanowires were also measured and showed rectifying behavior, in agreement with the measurements here, Figure 1b.[14,15,34,42] Pristine contacts have previously been shown to exhibit Schottky behavior when the Au particle is comparable in diameter to the nanowire.[15] The depletion region created by the Au is laterally constricted by the reduced interface size (typically ~80% of nanowire diameter) because of the necking that occurs at the edge of the contact interface. The effect of this laterally constricted depletion region are transport properties that are dominated by tunneling at the contact edge where the depletion layer is thin.[15] This effect is enhanced in the aged ohmic nanowires due to the additional defective ZnO at the interface edge.[14]

*Current–Voltage Limits and Stability of Ohmic Au Nanocontacts on ZnO Nanowires.* The same aged ohmic nanowires were then cycled with increasing voltage sweeps (±1 V to ±10 V) until the current reached several $\mu$A and the $I-V$ characteristics became symmetrical and "S-shaped". However, there was no indication of a dominant Schottky barrier at either end-contact of the nanowires in the current–voltage behavior, Figure 2a. Three nanowires (~55 nm diameter and ~300–450 nm cantilever length) were driven to failure caused by thermal breakdown[7] near the midpoint of the shaft when the current was ~10 $\mu$A. When Figure 2b,c are compared, the images show a typical example of an ohmic-type nanowire before and after breakdown. The current density at which the nanowires failed was 2.4 × $10^5$, 3.9 × $10^5$, and 6.1 × $10^5$ A $cm^{-2}$ that was seemingly dependent on the estimated resistivity at +1 V of 5.1, 0.75, and 0.64 Ωcm, respectively.

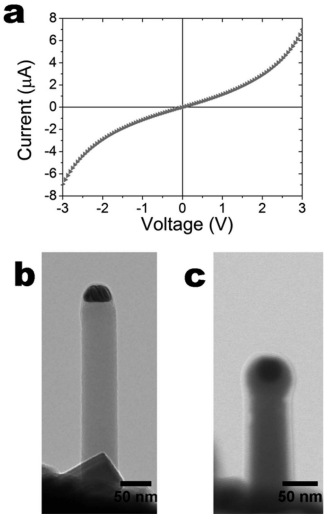


**Figure 2.** (a) $I-V$ graph of an aged nanowire at greater bias (±3 V) showing the near-linear transport characteristics. (b) Bright-field TEM image of the same nanowire before $I-V$ measurement. (c) SEM-STEM image of the same nanowire after breakdown when the voltage was increased beyond 3 V.

Failure at the midpoint is consistent with other semiconductor nanowire materials with low-resistance ohmic contacts where the maximum Joule heating effect occurs in the middle of the nanowire span away from the contacts that act as heatsinks.[6,7,52,53] Failure resulted in melting of the nanowire, leaving a ZnO stump with or without a bulblike ZnO end and a spherical Au nanoparticle, as shown by comparing Figure 2b,c. The remaining Au volume is estimated from geometrical considerations to be less than the original premeasurement volume indicating Au loss during breakdown. For the nanowires that were cycled to a current density (there was no apparent relationship between voltage and breakdown) just below this range (~1 × $10^5$–4 × $10^5$ A $cm^{-2}$ depending on resistivity) no degradation of the nanowire was observed with transmission SEM. In addition, the $I-V$ characteristics of these nanowires at ±1 V remained the same after the high current density measurements, indicating that no lasting change had occurred to the nanowires.

*Current–Voltage Limits and Stability of Schottky Au Nanocontacts on ZnO Nanowires.* In a similar fashion to the ohmic nanowires, the Schottky-type freshly grown nanowires were cycled with $I-V$ sweeps in ±0.1 V increments and the $I-V$ data was recorded at each step. The aberration-corrected STEM imaging in the initial state (Figure 3a) and $I-V$ data of the same Au–nanowire contact is shown in Figure 3 with the nanowire labeled Schottky 1 (~52 nm diameter). The $I-V$ graphs are divided (Figure 3b,d) into two distinct transitions in $I-V$ behavior. The initial $I-V$ graph for Schottky 1 (Figure 3b, labeled "$I-V$ Change") shows select data from the first ±1 V measurement up to ±5 V, and for comparison a post ±1 V measurement (red dashes-dots) is shown to highlight the change in the contact properties. It is evident from the data that the nanowire retained the same rectifying quality from ±1 to ±3 V with no change in the $I-V$ characteristics reaching −760 nA reverse-bias current at −3 V that equates to a current density of 6.7 × $10^4$ A $cm^{-2}$ for the 38 nm interface width. The voltage sweeps were incrementally increased and a change in reverse-bias characteristics was observed above ±3 V, as shown by the cyan curve of ±3.5 V (Figure 3b). The reverse bias current deviates from the original rectifying quality to greater current values as the voltage is increased. With increasing voltage sweeps the reverse bias current deviates further from the original rectifying properties as shown by the curves for ±4 (pink) and ±4.5 V (yellow), Figure 3b. This increase in reverse-bias current is indicative of quantum-mechanical tunneling current-induced breakdown at the interface and as our previous work has shown tunneling is concentrated at the interface edge.[14,15] When the voltage sweeps approached 5 V there is a dramatic increase in reverse bias current typical of reverse-bias breakdown of Schottky contacts; however, on closer examination of the ±5 V curve, hysteresis is also evident in reverse-bias indicating some permanent change of the interface has occurred where the current reaches a maximum of −20 $\mu$A (this wire shows increased current carrying capability compared to the Ohmic nanowires that is potentially a result of the heating effect occurring at the Au–ZnO interface that is in thermal contact with the measurement probe rather than at the midspan of the nanowires with Ohmic contacts). Hysteresis in $I-V$ characteristics is evidence of the trapping and releasing of charge carriers due to defects and is associated with tunneling through defect states.[54] The permanent change is confirmed by comparing (Figure 4b) the ±3 (blue) before and ±1 V (red dashes-dots) curves that show the contact has lost much of its rectifying quality and in reverse-bias the ±1 V $I-V$ behavior now traces that of the ±5 V curve. However, it is notable that there is no change in the forward-bias $I-V$ behavior for any of the $I-V$ sweeps in this initial stage of experiments and the


DOI: 10.1021/acs.nanolett.7b02561
Nano Lett. 2017, 17, 6626–6636

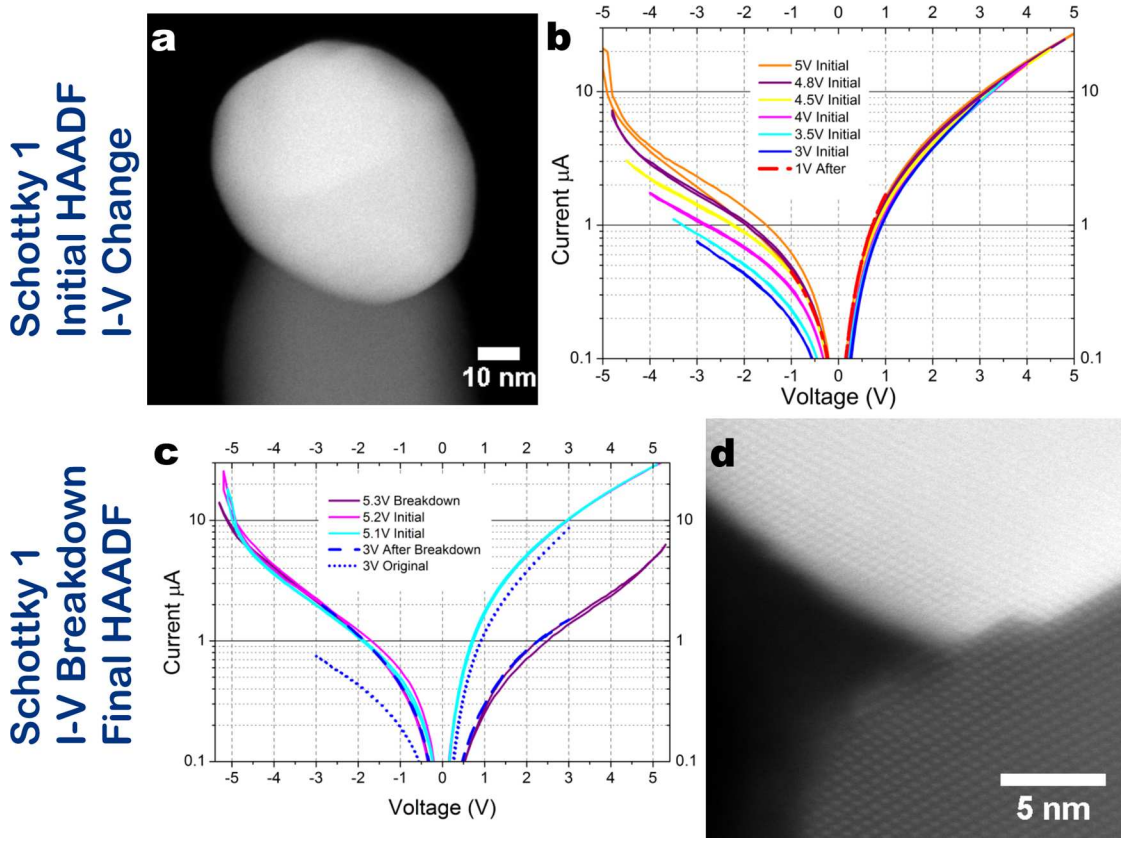


**Figure 3.** *I*–*V* graphs (b,d) for a Schottky-like nanowire (Schottky 1) correlated to HAADF images before (a) and after (d) the increasing voltage electrical measurements that show the initial *I*–*V* Change and then *I*–*V* breakdown of the contact as the voltage sweeps were increased in ±0.1 V steps. The final HAADF image (d) shows a double atomic step defect created at the Au–ZnO interface edge during the electrical breakdown.

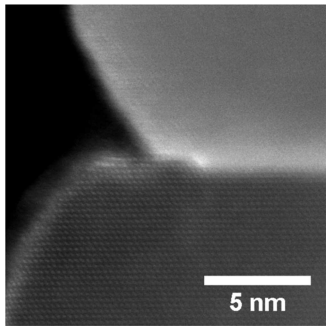


**Figure 4.** MAADF image of the double atomic Au step at the edge of Schottky 1 highlighting the strain that occurs at the interfacial defect that changes the local potential barrier at the interface edge.

nanowire retains the same forward-bias behavior when current transport is dominated by thermionic-emission over the potential barrier spreading the current across the entire interface area, rather than tunneling through the barrier in reverse-bias at the perimeter of the nanowire-nanocontact interface.[37] In this example, a noticeable change in reverse-bias current is observed when the current exceeds −760 nA (±3 V) for this nanowire that has approximately 52 nm diameter on the shaft with a similar Au diameter; however, there is always considerable narrowing at the interface because of the necking[15,50] creating an interface of 38 nm diameter.[15] Previous finite-element simulations have shown that edge-tunneling is the dominant cause of heating in Au–ZnO nanowire contacts and is localized at the contact edge perimeter and that the smaller the nanocontact interface, in comparison to the nanowire, the greater the heating effect because of the greater concentration of current.[46] Supporting Information Figure S13b shows that nearly identical behavior is exhibited by another nanowire Schottky 2 (labeled "*I*–*V* Change") with a change in reverse-bias rectification occurring above −3 V (−722 nA and interface current density of $6.4 \times 10^4$ A cm$^{-2}$) and increasing reverse-bias breakdown until hysteresis appears at 4.3 V at a reverse-bias current of −10 μA. The lower observed current when compared to Schottky 1 is due to the smaller diameter of the Schottky 2 nanowire (~43 nm). However, the lower current that induces hysteresis in the *I*–*V* characteristics of Schottky 2 actually occurs at an interfacial current density that is approximately equal to the reverse bias hysteresis-inducing Schottky 1 current density. The initial ±3 V and after ±1 V *I*–*V* sweeps for Schottky 2 confirm the permanent change in the rectifying behavior that is shown in Supporting Information Figure S13b for this initial stage of the measurements.

Schottky 1 and Schottky 2 were then measured with further voltage increments until there was an observed change in the forward-bias behavior (labeled "*I*–*V* Breakdown" for Schottky 1 in Figure 3c and Schottky 2, Figure S13c). For Schottky 1 the forward-bias *I*–*V* characteristics remained identical to the lower voltage ranges up to a value of 5.2 V (pink) while there is a dramatic increase in reverse-bias current beyond the −5 V range reaching values of −26 μA at −5.2 V. Increasing the *I*–*V* sweeps further, Schottky 1 then undergoes complete breakdown in *I*–*V* behavior when the voltage sweep is increased from ±5.2 to ±5.3 V and shows reverse-rectifying properties



DOI: 10.1021/acs.nanolett.7b02561
*Nano Lett.* 2017, 17, 6626–6636

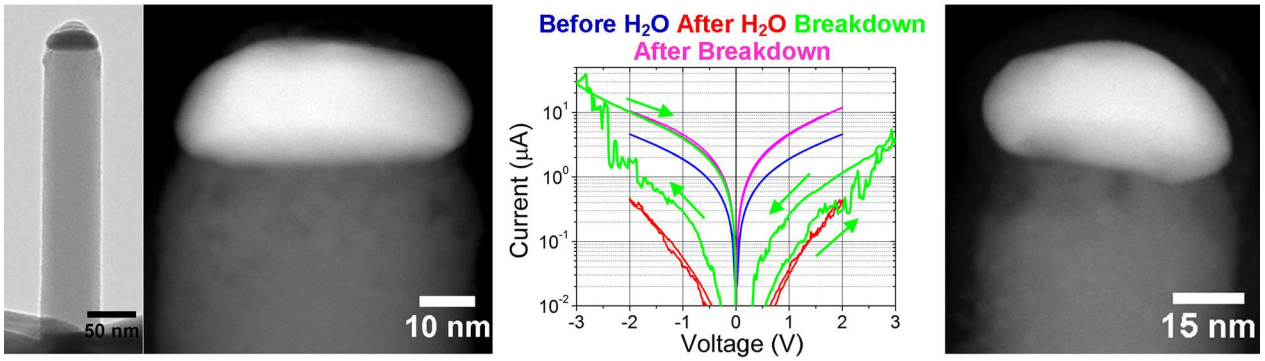


**Figure 5.** A ZnO nanowire with Au nanocontact that showed electrical breakdown in reverse bias after the etch treatment; from left to right: bright-field TEM image of the complete nanostructure and Au nanoparticle before measurement; HAADF ac-STEM image of the Au nanocontact and ZnO nanowire showing the chronologically degraded near-interface region; *I*−*V* data before (blue) and after etching (red) with deionized $H_2O$, and during (green) and after breakdown (purple); HAADF ac-STEM image after etching and electrical breakdown measurement.

(Figure 3c, purple curve) that have previously been observed in defective etched Au−ZnO nanowire contacts.[14] A reduction from ∼30 μA at +5.2 V to ∼6 μA at +5.3 V occurs as the contact undergoes complete breakdown while the reverse bias characteristics remain similar but with a reduction in current from −26 μA at −5.2 V to −14 μA at −5.3 V. The permanent change is confirmed by the voltage sweeps of ±1 to ±3 V after breakdown has occurred (see the ±3 V blue dashed curve in Figure 3c labeled Schottky 1 *I*−*V* breakdown and the initial original-state ±3 V *I*−*V* curve (dots) is included for comparison). The same breakdown and change to reverse rectifying properties is observed in Schottky 2 when the voltage sweeps are increased from ±5 to ±5.4 V with a reduction in forward-bias current at 5.3 V of ∼17 to 0.3 μA at 5.4 V (see Figure S13c that shows *I*−*V* data between ±5 and ±5.4 V along with select post breakdown data confirming the permanent change to reverse-rectifying properties,).

The final ac-STEM analysis of both Schottky 1 and Schottky 2 shown in Figure 3d and Supporting Information Figure S13d, respectively, labeled *I*−*V* Breakdown, reveal the evidence of atomic Au steps that occur near the edge of the Au−ZnO interface where tunneling current is at a maximum. In contrast to the earlier discussions on Au steps at the interface of twinned Au particles at the ZnO interface, the steps in Schottky 1 and Schottky 2 after breakdown occur at the Au−ZnO edge where no Au twins are present. This suggests the steps are modifications to the interface that have occurred to the Au−ZnO interface as a result of the *I*−*V* measurements leading to the observed changes and eventual breakdown in transport properties. Figure 4 shows a MAADF image of a postmeasurement Au step of Schottky 1. Because of the smaller inner collection angle of this detector, strained and defected areas produce brighter contrast in MAADF images, chiefly due to dechanneling of the electrons which are then scattered to intermediate angles. In Figure 4, additional bright contrast highlights the strain present at the double atomic-layer Au defect step created due to the modification of the Au−ZnO interface.[55] Increased strain and changes in bond formation at a metal−semiconductor interface cause local changes to the potential barrier creating barrier inhomogeneity that occurs in these nanowires at the tunneling channel located at the interface edge for Schottky 1 and Schottky 2 where the majority of the current is concentrated.[47,56] Introduced impurities, defects, and structural anomalies at or near the interface could potentially change the transport properties from the initial Schottky behavior to the observed transitional Ohmic transport characteristics. Such effects have been covered over many decades by eminent researchers both theoretically and experimentally.[37,47] However, the Au−nanowire system provides a major advantage in that the interface can be interrogated at the atomic level both structurally and chemically. The doping effect of a single Au atom within the ZnO matrix near to the interface is unknown but would be expected to introduce some effect of barrier inhomogeneity. In the nanowires studied here the predominance of edge tunneling can exclude this influence of an Au atom unless it was located in the ZnO lattice near to the interface edge where the tunneling current is concentrated. For this reason, our previous work studied the Au−ZnO interfaces with aberration-corrected HAADF imaging and through-focal sectioning correlated to multislice simulations to determine the sensitivity of the technique for "Z-contrast" detection of a single Au atom within the ZnO lattice.[50] The analysis and simulations determined that a single Au atom would provide sufficient contrast such that it could be detected with HAADF imaging while even taking into consideration channeling effects and other hindrances to Z-contrast imaging. The multislice simulations showed that for a ZnO slab of thickness 7 nm a Z-contrast increase of 20% could be expected over that of the hoist ZnO lattice while for a thicker slab of 14 nm a contrast increase of 15% would be expected. The simulations considered the ZnO in the $[01\bar{1}0]$ zone axis orientation. The nanowire labeled Schottky 1 in Figure 4 is orientated on the zone axis $[1\bar{2}10]$ and thus the flat $\{01\bar{1}0\}$ side facets are parallel to the beam. Given this nanowire has an Au−ZnO interface width of ∼38 nm geometrical considerations provide the maximum expected thickness of ZnO at the interface edge will be ∼22 nm. However, substantial interrogation of the Au−ZnO structures always shows considerable necking of the ZnO near the metal interface with the crystallographic facets providing a range of angles with the metal particle interface. The nanowire top facets around the Au contact have been determined on inspection with STEM/HAADF/TEM imaging and SAED patterns to be the sloping facets in the range between $\{2\bar{1}\bar{1}4\}$ and $\{1\bar{1}01\}$ that extend from the nanowire $\{01\bar{1}0\}$ side facets to join the Au contact interface and (0001) nanowire top facet.[15] This crystallographic formation is expected to create substantially thinner facets than the side $\{01\bar{1}0\}$ that extend the length of the nanowire shaft. Therefore, within the limits of the techniques and simulations



DOI: 10.1021/acs.nanolett.7b02561
*Nano Lett.* 2017, 17, 6626−6636

available we can state that single Au atoms were not detected in the critical edge region in the ZnO matrix.

The final breakdown change to reverse-rectification indicates increased defect-induced tunneling through the potential barrier which is confirmed by the presence of three step edges present on Schottky 1 (Figure S14). Schottky 2 only shows modification of the interface in one location but with multiple Au lattice planes at the Au−ZnO edge (Figure S13d). This difference in Au step formation of Schottky 1 and Schottky 2 is likely to be a contributing factor to the slight variations in $I-V$ behavior before the final breakdown and may indicate the formation of the defects was an ongoing process as the voltage was increased to the ultimate transformation in transport behavior to reverse-rectifying characteristics.

*Current−Voltage Limits and Stability of Edge-Modified Au Nanocontacts on ZnO Nanowires.* In comparison, to test the electrical limits of edge-modified contacts that had the edge-tunneling path removed by $H_2O$ etching,[14] eSTEM nanowires were measured with voltage sweeps greater than ±2 V and resulted in greater current across the contacts that eventually displayed breakdown characteristics with a large jump in current in reverse bias (see green curve in Figure 5). Following breakdown, the contact in Figure 5 had reverted to a highly conductive ohmic contact, exhibiting similar $I-V$ characteristics to the original measurement (pink and blue curves, respectively in Figure 5).

In this example, the current increased to −30 μA in magnitude during reverse bias breakdown, equivalent to a current density of ∼$1.1 \times 10^6$ A $cm^{-2}$, slightly greater than the current density that led to the chronologically aged ohmic nanowire breakdown in the central portion of the shaft but of similar magnitude to the Schottky nanowires which is again partially due to the initial-state resistivity being considerably lower for this nanowire (0.45 Ωcm compared to 0.64 Ωcm for the previous lowest resistivity ohmic nanowires and this nanowire had a larger 60 nm diameter). However, the etched contact initially began the $I-V$ transformation in forward-bias creating the forward-bias hysteresis shown in the graph (green curve, Figure 5) when the current (∼4 μA) was distributed across the interface and transport was dominated by emission over the barrier. Transport across the etched contacts is determined by the nature of the central Au−ZnO interface rather than the edge-tunneling that dominates the ohmic and Schottky contacts. Complete and irreversible breakdown occurred in reverse-bias when the transport was tunneling dominated through the central zone of the contact potential barrier leading to heating and structural breakdown. The permanent change in the contact properties resulted in the current rapidly escalating to −30 μA during the measurement. For the etched nanowires, the central Au−ZnO interface becomes the current-limiter because of the removal of the tunneling channel creating reduced interface conductivity that leads to breakdown at the contact rather than the nanowire shaft. Previous finite-element simulations of nonaged Au nanocontacts to ZnO nanowires have shown that metal nanocontact (24 nm interface diameter) melting occurs at 1064 °C on a perfect ZnO nanowire when the current exceeds ∼10 μA, in good agreement with the measurements on all of the etched nanowires measured here and the formation of interfacial defects in the Schottky nanowires.[46] In situ TEM heating experiments (Figure S15) of the Au−ZnO nanowires show that the Au particle remains solid and the ZnO nanowires are stable to temperatures of at least ∼800 °C, providing additional evidence that high current densities that may cause heating effects should not adversely affect the overall structure of the materials that is essential for an operational device in extreme environments.

Examining the ac-STEM images in Figure 5 shows that the Au has undergone a distinct change in configuration with respect to the nanowire and appears to have evolved in shape (the HAADF images in Figure 5 appear to show the Au has changed shape with additional faceting but this is not conclusive due to projection effects) due to the very high current experienced during breakdown and the analysis also provides indications that that the ZnO has changed density near the interface. The contact heating changed the etched contact's transport properties to low-resistance and ohmic-like while the annealing effect reverted the resistance of the nanowire to a similar state to the original resistance before etching.

The measurements here have shown that the characteristics of irreversible breakdown of the Au−ZnO nanowires are dictated by the balance of nanowire and contact interface conductivity. Initially, when the Au−nanowire contacts were ohmic and low-resistance, breakdown occurred at the midpoint of the nanowire shaft. Failure at the interface of the Au contacts occurred when the Au−ZnO interface was degraded with "high-resistance" or displayed Schottky-type characteristics, creating maximum heating effects at the Schottky contact rather than at the nanowire midpoint creating atomic-scale interfacial defects near to the contact edge where tunneling current, and therefore heating, is concentrated.

**Conclusion.** We have shown that the electrical transport properties of Au nanocontacts to ZnO nanowires are dominated by the structure of the semiconductor at the contact edge and the structures are stable and robust components for many devices. Aged ohmic Au−ZnO nanowires show typical breakdown at the nanowire midshaft while high resistance etched and pristine Schottky Au−ZnO contacts reveal breakdown occurs at the metal−semiconductor interface. The measurements showed the Schottky nanowires are robust components up to ±3 V and reverse-bias tunneling of ∼−1 μA and can withstand long periods of electrical stress. Fascinatingly, the ac-STEM analysis revealed atomic-scale defects at the interface edge of the Schottky-type nanowires that were a result of the concentration of tunneling current at the contact perimeter. The work confirms Au−ZnO nanocatalyst structures are ideal candidates for a multitude of single-nanowire devices with tailorable properties. The new concepts shown here provide interesting possibilities for bridged nanowire devices such as transient electronics and reactive circuit breakers that respond to changes in electrical signals or environmental factors and provide instantaneous reactions to electrical overload.

**Experimental and Methods.** *Sample Preparation.* ZnO nanowires were grown via a high-temperature vapor-phase method that used a thin 5 nm Au layer on the sapphire substrate to initiate growth and provide the one-step electrical nanocontacts on the nanowire tips. Lattice matched sapphire ($1\bar{1}20$) was used to grow the nanowires in vertical arrays with single crystal quality.[33] To allow electrical probing of the nanowires and subsequent electron microscopy the nanowires were mechanically transferred to the fingers of standard FIB lift-out copper grids (Omniprobe). The application of a standard TEM grid avoided restrictions on tilting degrees of freedom that some in situ TEM-STM modules can present providing the distinct advantage that many nanowires could be aligned to a



DOI: 10.1021/acs.nanolett.7b02561
Nano Lett. 2017, 17, 6626−6636

crystallographic axis such that the metal−semiconductor junction was parallel to the beam. Fabrication of additional measurement contacts that are required for "on-chip" in situ measurement devices was not necessary ensuring the nanowire surface, nanowire structure, and Au−ZnO interface were not unintentionally modified before measurement. Nanowires in the array configuration and on the grids were screened with a Hitachi S4800 SEM using the secondary electron and backscattered electron detectors. Nanowire grid samples were also screened with a Tecnai TF20 with bright-field imaging. Etching was performed after 2 min $O_2$ plasma cleaning before dipping the nanowires in deionized water for 5 min that were then immediately vacuum-dried. The extent of the etching was optimized on similar nanowires that were inspected with SEM.[14]

*Electrical Transport Measurement.* The nanowires that were in the eSTEM cantilever configuration on the lift-out grids were loaded in the chamber of an UHV Omicron LT Nanoprobe. The tungsten STM probes that had been thermally annealed[35] were manually lowered to the height of the horizontal nanowires using the focal plane of the in situ SEM. With a small applied bias of 0.2 V, one probe was brought into contact with the Au particle at the tip of the nanowire using real-time current feedback. The sample grid was at the low potential throughout the measurements. Once a signal above the noise was detected the SEM beam was turned off and the bias was incrementally ramped at 10 s intervals to the desired current. The desired current was maintained for up to 15 min and then the voltage was ramped down to 0 V and the probe was carefully removed from the contact position. *I*−*V* sweeps of the same nanowires were performed in a similar manner using a Keithley 2636 sourcemeter. *I*−*V* sweeps using the two-probe method were performed in a similar fashion that has previously been described.[15,34,42] The removal of probe oxides and contamination was confirmed by testing the resistance between the tips of two measurement probes (∼200 Ω) and between the probe and grid (∼300 Ω) which are comparable to the resistance of the measurement system (∼120 Ω).

*Aberration-Corrected STEM.* High-resolution HAADF, (MAADF, and bright-field imaging was carried out in a Nion UltraSTEM100 STEM operated at 100 keV primary beam energy that was equipped with an UHV Enfina EELS spectrometer. The probe-forming optics, corrected for aberrations up to fifth order, were configured to provide ∼50 pA of beam current with a 31 mrad beam convergence semiangle, for an estimated probe size of 0.8 Å. The inner and outer radii of the HAADF detector were calibrated at 79 and 195 mrad, respectively, and of the MAADF 40 and 86 mrad, respectively (when used simultaneously with the HAADF). Using this technique, nanowires were tilted to an available zone axis of the nanowire or Au particle and the structure was imaged using phase contrast, MAADF, and HAADF imaging. To ensure minimal beam damage of the structures core-loss electron energy loss spectroscopy (EELS) was carried out after the initial imaging and electrical assessment. Compositional EELS mapping was performed using the same beam configuration using 100 keV primary beam energy and an exposure of 0.06 s per pixel. Chemical maps were created by integrating over a suitable energy window the intensity above the relevant EELS edges (Zn−$L_{2,3}$, O−K, C−K, and Au−$M_{4,5}$) after removal of the decaying background using a power law model. The EELS data was systematically denoised using principal component analysis. Noise-reduction frame averaging and rigid registration[57] was performed using a Digital Micrograph script "Smart-Alignment," by D. R. G. Mitchell, adminnospam@dmscripting.com version: 20150524, v2.0, May 2015, and SmartAlign.[58]

*In Situ TEM Heating of Nanowires.* Heating of the Au−ZnO structures was performed in a Hitachi H-9000 UHV TEM operated at 300 keV. The nanowires were mechanically transferred onto a silicon chip that contained a window composed of 50 nm thick silicon nitride. After loading into the microscope vacuum system, the sample was baked at 100 °C in the loadlock then transferred to the microscope polepiece. It was then heated gradually to 800 °C in an oxygen pressure of $1 \times 10^{-6}$ Torr while recording 30 images per second under bright-field conditions. Resistive heating via direct current was used with the temperature-current relationship measured with an infrared pyrometer after the experiment. We estimate an accuracy of ±20 °C in the temperature values quoted.

## ■ ASSOCIATED CONTENT

### Supporting Information

The Supporting Information is available free of charge on the ACS Publications website at DOI: 10.1021/acs.nanolett.7b02561.

Additional data: ac-STEM microscopy, EELS, experimental *I*−*V* data, and in situ TEM heating images; detailed descriptions of the experimental measurement process and nanowire properties (PDF)

## ■ AUTHOR INFORMATION


### Corresponding Author

*E-mail a.m.lord@swansea.ac.uk.

### ORCID

Alex M. Lord: 0000-0002-6258-2187

Despoina M. Kepaptsoglou: 0000-0003-0499-0470


### Author Contributions

The manuscript was written through contributions of all authors. All authors have given approval to the final version of the manuscript.

### Notes

The authors declare no competing financial interest.

## ■ ACKNOWLEDGMENTS

A.M.L. would like to thank the support of the Sêr Cymru II fellowship scheme part-funded by the European Regional Development Fund through the Welsh Government. This work was supported by the Centre for Nanohealth, Swansea University, U.K. Aberration-corrected STEM analysis was performed at the SuperSTEM Laboratory, the U.K. National Facility for Aberration-Corrected STEM, funded by the EPSRC. Support was provided by the Engineering and Physical Sciences Research Council-funded Impact Acceleration Account [Grant EP/K504002/1]. TEM characterization data was enabled via support from the EPSRC funded Leeds EPSRC Nanoscience and Nanotechnology Equipment Facility (LENNF) (Grant EP/K023853/1) and ERC Grant 279342: InSituNANO. A.M.L. would like to thank Frances M. Ross for enabling the in situ TEM experiments and providing essential support and advice.



DOI: 10.1021/acs.nanolett.7b02561
*Nano Lett.* 2017, 17, 6626−6636

## REFERENCES


(1) Grosse, K. L.; Bae, M.-H.; Lian, F.; Pop, E.; King, W. P. *Nat. Nanotechnol.* **2011**, *6*, 287−90.
(2) Liu, Q.; Zou, R.; Wu, J.; Xu, K.; Lu, A.; Bando, Y.; Golberg, D.; Hu, J. *Nano Lett.* **2015**, *15*, 2809−2816.
(3) Fauske, V. T.; Huh, J.; Divitini, G.; Dheeraj, D. L.; Munshi, A. M.; Ducati, C.; Weman, H.; Fimland, B.-O.; van Helvoort, A. T. J. *Nano Lett.* **2016**, *16*, 3051−3057.
(4) Alam, S. B.; Panciera, F.; Hansen, O.; Mølhave, K.; Ross, F. M. *Nano Lett.* **2015**, *15*, 6535−6541.
(5) Panciera, F.; Norton, M. M.; Alam, S. B.; Hofmann, S.; Mølhave, K.; Ross, F. M. *Nat. Commun.* **2016**, *7*, 12271.
(6) Westover, T.; Jones, R.; Huang, J. Y.; Wang, G.; Lai, E.; Talin, A. A. *Nano Lett.* **2009**, *9*, 257−263.
(7) Zhao, J.; Sun, H.; Dai, S.; Wang, Y.; Zhu, J. *Nano Lett.* **2011**, *11*, 4647−4651.
(8) Zhang, C.; Neklyudova, M.; Fang, L.; Xu, Q.; Wang, H.; Tichelaar, F. D.; Zandbergen, H. W. *Nanotechnology* **2015**, *26*, 155703.
(9) Chen, R.; Jungjohann, K. L.; Mook, W. M.; Nogan, J.; Dayeh, S. A. *Nano Lett.* **2017**, *17*, 2189−2196.
(10) Baloch, K. H.; Voskanian, N.; Bronsgeest, M.; Cumings, J. *Nat. Nanotechnol.* **2012**, *7*, 316−319.
(11) Xu, Z.; Golberg, D.; Bando, Y. *Nano Lett.* **2009**, *9*, 2251−2254.
(12) Tang, D. M.; Ren, C. L.; Lv, R.; Yu, W. J.; Hou, P. X.; Wang, M. S.; Wei, X.; Xu, Z.; Kawamoto, N.; Bando, Y.; Mitome, M.; Liu, C.; Cheng, H. M.; Golberg, D. *Nano Lett.* **2015**, *15*, 4922−4927.
(13) Wang, Z.; Santhanagopalan, D.; Zhang, W.; Wang, F.; Xin, H. L.; He, K.; Li, J.; Dudney, N.; Meng, Y. S. *Nano Lett.* **2016**, *16*, 3760−3767.
(14) Lord, A. M.; Ramasse, Q. M.; Kepaptsoglou, D. M.; Evans, J. E.; Davies, P. R.; Ward, M. B.; Wilks, S. P. *Nano Lett.* **2017**, *17*, 687−694.
(15) Lord, A. M.; Maffeis, T. G.; Kryvchenkova, O.; Cobley, R. J.; Kalna, K.; Kepaptsoglou, D. M. D.; Ramasse, Q. M.; Walton, A. S.; Ward, M. B.; Köble, J.; Wilks, S. P. *Nano Lett.* **2015**, *15*, 4248−4254.
(16) Suyatin, D. B.; Jain, V.; Nebol'sin, V. a; Tragardh, J.; Messing, M. E.; Wagner, J. B.; Persson, O.; Timm, R.; Mikkelsen, A.; Maximov, I.; Samuelson, L.; Pettersson, H. *Nat. Commun.* **2014**, *5*, 3221.
(17) Léonard, F.; Talin, A.; Swartzentruber, B.; Picraux, S. *Phys. Rev. Lett.* **2009**, *102*, 106805.
(18) Hui, H. Y.; Filler, M. A. *Nano Lett.* **2015**, *15*, 6939−6945.
(19) Faraz, T.; Roozeboom, F.; Knoops, H. C. M.; Kessels, W. M. M. *ECS J. Solid State Sci. Technol.* **2015**, *4*, N5023−N5032.
(20) Gamalski, A. D.; Tersoff, J.; Kodambaka, S.; Zakharov, D. N.; Ross, F. M.; Stach, E. A. *Nano Lett.* **2015**, *15*, 8211−8216.
(21) Jacobsson, D.; Panciera, F.; Tersoff, J.; Reuter, M. C.; Lehmann, S.; Hofmann, S.; Dick, K. A.; Ross, F. M. *Nature* **2016**, *531*, 317−322.
(22) No, Y.-S.; Gao, R.; Mankin, M. N.; Day, R. W.; Park, H.-G.; Lieber, C. M. *Nano Lett.* **2016**, *16*, 4713−4719.
(23) Webb, J. L.; Knutsson, J.; Hjort, M.; Gorji Ghalamestani, S.; Dick, K. A.; Timm, R.; Mikkelsen, A. *Nano Lett.* **2015**, *15*, 4865−4875.
(24) Kempa, T. J.; Kim, S.-K.; Day, R. W.; Park, H.-G.; Nocera, D. G.; Lieber, C. M. *J. Am. Chem. Soc.* **2013**, *135*, 18354−18357.
(25) Ahvenniemi, E.; Akbashev, A. R.; Ali, S.; Bechelany, M.; Berdova, M.; Boyadjiev, S.; Cameron, D. C.; Chen, R.; Chubarov, M.; Cremers, V.; Devi, A.; Drozd, V.; Elnikova, L.; Gottardi, G.; Grigoras, K.; Hausmann, D. M.; Hwang, C. S.; Jen, S.-H.; Kallio, T.; Kanervo, J.; Khmelnitskiy, I.; Kim, D. H.; Klibanov, L.; Koshtyal, Y.; Krause, A. O. I.; Kuhs, J.; Kärkkänen, I.; Kääriäinen, M.-L.; Kääriäinen, T.; Lamagna, L.; Łapicki, A. A.; Leskelä, M.; Lipsanen, H.; Lyytinen, J.; Malkov, A.; Malygin, A.; Mennad, A.; Militzer, C.; Molarius, J.; Norek, M.; Özgit-Akgün, Ç.; Panov, M.; Pedersen, H.; Piallat, F.; Popov, G.; Puurunen, R. L.; Rampelberg, G.; Ras, R. H. A.; Rauwel, E.; Roozeboom, F.; Sajavaara, T.; Salami, H.; Savin, H.; Schneider, N.; Seidel, T. E.; Sundqvist, J.; Suyatin, D. B.; Törndahl, T.; van Ommen, J. R.; Wiemer, C.; Ylivaara, O. M. E.; Yurkevich, O. *J. Vac. Sci. Technol., A* **2017**, *35*, 10801.
(26) Zhang, C.; Miao, X.; Mohseni, P.; Choi, W.; Li, X. *Nano Lett.* **2014**, *14*, 6836.
(27) Liu, X.; Liu, M. H.; Luo, Y. C.; Mou, C. Y.; Lin, S. D.; Cheng, H.; Chen, J. M.; Lee, J. F.; Lin, T. S. *J. Am. Chem. Soc.* **2012**, *134*, 10251−10258.
(28) Kodambaka, S.; Tersoff, J.; Reuter, M. C.; Ross, F. M. *Phys. Rev. Lett.* **2006**, *96*, 96105.
(29) Hofmann, S.; Sharma, R.; Wirth, C. T.; Cervantes-Sodi, F.; Ducati, C.; Kasama, T.; Dunin-Borkowski, R. E.; Drucker, J.; Bennett, P.; Robertson, J. *Nat. Mater.* **2008**, *7*, 372−5.
(30) Kirkham, M.; Wang, X.; Wang, Z. L.; Snyder, R. L. *Nanotechnology* **2007**, *18*, 365304.
(31) Panciera, F.; Chou, Y.-C.; Reuter, M. C.; Zakharov, D.; Stach, E. A.; Hofmann, S.; Ross, F. M. *Nat. Mater.* **2015**, *14*, 820−825.
(32) Fu, K. K.; Wang, Z.; Dai, J.; Carter, M.; Hu, L. *Chem. Mater.* **2016**, *28*, 3527−3539.
(33) Yang, P.; Yan, H.; Mao, S.; Russo, R.; Johnson, J.; Saykally, R.; Morris, N.; Pham, J.; He, R.; Choi, H.-J. *Adv. Funct. Mater.* **2002**, *12*, 323−331.
(34) Lord, A. M.; Ward, M. B.; Evans, J. E.; Davies, P. R.; Smith, N. A.; Maffeis, T. G.; Wilks, S. P. *J. Phys. Chem. C* **2014**, *118*, 21177−21184.
(35) Cobley, R. J.; Brown, R. A.; Barnett, C. J.; Maffeis, T. G. G.; Penny, M. W. *Appl. Phys. Lett.* **2013**, *102*, 023111.
(36) Smith, N. A.; Lord, A. M.; Evans, J. E.; Barnett, C. J.; Cobley, R. J.; Wilks, S. P. *Semicond. Sci. Technol.* **2015**, *30*, 065011.
(37) Rhoderick, E. H.; Williams, R. H. *Metal-Semiconductor contacts*; Clarendon Press: Oxford, 1988.
(38) Ramasse, Q. M. *Ultramicroscopy* **2017**, *180*, 41.
(39) Timm, R.; Persson, O.; Engberg, D. L. J.; Fian, A.; Webb, J. L.; Wallentin, J.; Jönsson, A.; Borgström, M. T.; Samuelson, L.; Mikkelsen, A. *Nano Lett.* **2013**, *13*, 5182−5189.
(40) Storm, K.; Halvardsson, F.; Heurlin, M.; Lindgren, D.; Gustafsson, A.; Wu, P. M.; Monemar, B.; Samuelson, L. *Nat. Nanotechnol.* **2012**, *7*, 718−722.
(41) Fian, A.; Lexholm, M.; Timm, R.; Mandl, B.; Håkanson, U.; Hessman, D.; Lundgren, E.; Samuelson, L.; Mikkelsen, A. *Nano Lett.* **2010**, *10*, 3893−3898.
(42) Lord, A. M.; Walton, A. S.; Maffeis, T. G.; Ward, M. B.; Davies, P.; Wilks, S. P. *Nanotechnology* **2014**, *25*, 425706.
(43) Lord, A. M.; Maffeis, T. G.; Allen, M. W.; Morgan, D.; Davies, P. R.; Jones, D. R.; Evans, J. E.; Smith, N. A.; Wilks, S. P. *Appl. Surf. Sci.* **2014**, *320*, 664−669.
(44) Qin, W.; Hou, J.; Bonnell, D. A. *Nano Lett.* **2015**, *15*, 211−217.
(45) Smit, G. D. J.; Rogge, S.; Klapwijk, T. M. *Appl. Phys. Lett.* **2002**, *81*, 3852−3854.
(46) Kryvchenkova, O.; Kalna, K.; Cobley, R. J. Modelling heating effects due to current crowding in ZnO nanowires with end-bonded metal contacts. *Conf. Proc. - 10th Int. Conf. Adv. Semicond. Devices Microsystems, ASDAM 2014*, Smolenice, Slovakia, 2014; pp 1−4. DOI: 10.1109/ASDAM.2014.6998695.
(47) Tung, R. *Phys. Rev. B: Condens. Matter Mater. Phys.* **1992**, *45*, 13509−13523.
(48) Hou, J.; Nonnenmann, S. S.; Qin, W.; Bonnell, D. A. *Adv. Funct. Mater.* **2014**, *24*, 4113−4118.
(49) Brewster, M. M.; Zhou, X.; Lim, S. K.; Gradečak, S. *J. Phys. Chem. Lett.* **2011**, *2*, 586−591.
(50) Lord, A. M.; Maffeis, T. G.; Walton, A. S.; Kepaptsoglou, D. M.; Ramasse, Q. M.; Ward, M. B.; Köble, J.; Wilks, S. P. *Nanotechnology* **2013**, *24*, 435706.
(51) Van Benthem, K.; Lupini, A. R.; Oxley, M. P.; Findlay, S. D.; Allen, L. J.; Pennycook, S. J. *Ultramicroscopy* **2006**, *106*, 1062−1068.
(52) LeBlanc, S.; Phadke, S.; Kodama, T.; Salleo, A.; Goodson, K. E. *Appl. Phys. Lett.* **2012**, *100*, 163105.
(53) Wurz, J.; Logeeswaran, V. J.; Sarkar, A.; Islam, M. S. In *2008 8th IEEE Conference on Nanotechnology*; IEEE Conference Publications, 2008; pp 595−597.
(54) Yengui, M.; Riedel, D. *J. Phys. Chem. C* **2015**, *119*, 22700−22708.
(55) Yu, Z.; Muller, D. A.; Silcox, J. *J. Appl. Phys.* **2004**, *95*, 3362−3371.




DOI: 10.1021/acs.nanolett.7b02561
*Nano Lett.* 2017, 17, 6626−6636

(56) Mosbacker, H. L.; Zgrabik, C.; Hetzer, M. J.; Swain, A.; Look, D. C.; Cantwell, G.; Zhang, J.; Song, J. J.; Brillson, L. J. *Appl. Phys. Lett.* **2007**, *91*, 072102.
(57) Kimoto, K.; Asaka, T.; Yu, X.; Nagai, T.; Matsui, Y.; Ishizuka, K. *Ultramicroscopy* **2010**, *110*, 778−782.
(58) Jones, L.; Yang, H.; Pennycook, T. J.; Marshall, M. S. J.; Van Aert, S.; Browning, N. D.; Castell, M. R.; Nellist, P. D. *Adv. Struct. Chem. Imaging* **2015**, *1*, 8.



DOI: 10.1021/acs.nanolett.7b02561
*Nano Lett.* 2017, 17, 6626−6636